Journal of Solid State Chemistry

Volume 197, Pages 1-566 (January 2013)

Highlights

► Reaction process in the preparation of $Cu_2Al_6B_4O17$ whiskers was researched systematically.

► Crystal growth mechanism of $Cu_2Al_6B_4O17$ whiskers was proposed by theory and experiments.

► Properties of $Cu_2Al_6B_4O17$ were analyzed by instruments, such as TG-DSC, ICP-AES, XRD and SEM.

Tm(III)-succinate

Original Research Article
Pages 7-13
Carlos Alberto F. de Oliveira, Fausthon Fred da Silva, Ivani Malvestiti, Valéria Rodrigues dos S. Malta, José Diogo L. Dutra, Nivan B. da Costa Jr., Ricardo O. Freire, Severino A. Júnior

Highlights

► Was synthesized new MOFs based on Tm^{3+} ions and succinic acid in different temperature. ► The change in the temperature leads to two compounds with different crystalline systems. ► The Sparkle AM1, PM3 and PM6 models were used to comparison of the theoretical and experimental cell.

Co-Al mixed metal oxides/carbon nanotubes nanocomposite prepared via a precursor route and enhanced catalytic property

Original Research Article
Pages 14-22
Guoli Fan, Hui Wang, Xu Xiang, Feng Li

Highlights

► Co-Al mixed metal oxides/carbon nanotubes nanocomposite was synthesized. ► Co-Al mixed metal oxides consisted of cobalt oxide and Co-containing spinels.► Nanocomposite exhibited excellent catalytic activity for the decomposition of AP. ► The superior catalytic property is related to novel heterostructure and composition.

Synthesis of superhydrophobic SiO_2 layers via combination of surface roughness and fluorination

Original Research Article
Pages 23-28
Eun-Kyeong Kim, Ji Yeong Kim, Sang Sub Kim

Highlights

► Superhydrophobic SiO_2 layers are realized by a combination of surface roughness and fluorination. ► The fluorinated rough SiO_2 layer shows enhanced repellency toward various liquid droplets. ► The wetting behavior is explained based on Cassie-Baxter and Young-Dupre equations. ► The superhydrophobic SiO_2 layers confirm a promising practical application.

Carbon spheres-assisted strategy to prepare mesoporous manganese dioxide for supercapacitor applications

Original Research Article
Pages 29-37
Siheng Li, Li Qi, Lehui Lu, Hongyu Wang

Highlights

► Mesoporous MnO_2 was prepared by *in-situ* redox method assisted by carbon spheres. ► S_{BET}, pore size and volume were higher than MnO_2 obtained without carbon spheres. ► They could function well when used as electrode materials for supercapacitor. ► Ideal capacitive behaviors and long cycling life showed after 2000 charge-discharge.

Oxygen nonstoichiometry and thermo-chemical stability of La0.6Sr0.4CoO 3-й

Original Research Article
Pages 38-45
M. Kuhn, S. Hashimoto, K. Sato, K. Yashiro, J. Mizusaki

Highlights

► Oxygen nonstoichiometry of La0.6Sr0$_4$CoO $_3$-^ at intermediate temperatures and *p(O2).* ► Experimental confirmation of previously interpolated reduction enthalpy. ► Decomposition

p(O2) assessed by coulometric titration. ► Hysteresis-like *p(O2)* dependence of oxygen content at decomposition *p(O2).*

Two new metal-organic coordination polymers of lead with O-, N-donor ligands: Synthesis, characterization, luminescence and thermal behavior

Original Research Article
Pages 46-52
Abhinandan Rana, Swapan Kumar Jana, Madhusudan Bera, Debdoot Hazari, Durga Sankar Chowdhuri, Ennio Zangrando, Sudipta Dalai

Highlights

► 3-hydroxypicolinic acid is used for first time with Pb^{2+} in a MOF. ► 5-sulfoisophthalic acid displays two novel binding modes of high denticity. ► Complex **1** shows high thermal stability (up to 167 °C). ► MLCT is present in both the complexes.

Surfactant-assisted synthesis of hybrid lithium iron phosphate nanoparticles for enhancing electrochemical performance

Original Research Article
Pages 53-59
Jung Min Kim, Gi-Ra Yi, Soon Chang Lee, Sang Moon Lee, Younghun Jo, Hyun-Wook Kang, Gaehang Lee, Hae Jin Kim

Highlights

► $LiFePO_4$ nanohybrids are synthesized through the organic-inorganic co-assembly method. ► Copolymers (F108 or P123) serve as structure directing agents and a carbon source. ► P123 produces more graphitic carbon and higher crystalline nanohybrids. ► Nanohybrids using P123 show superior rate capability in Li-ion battery.

Synthesis, structural and electrical properties of $[C_2H10N_2]$ $[(SnCl(NCS)_2]_2$

Original Research Article
Pages 60-68
Sahel Karoui, Slaheddine Kamoun, Amor Jouini

Highlights

► X-ray diffraction analysis shows the 1D network character of the structure. ► DSC experiments show a phase transition at 336 K. ► The AC conductivity is interpreted in terms of Jonsher's law. ► Two conduction mechanisms are proposed for phase I and II.

Controllable synthesis of ZnO nanograss with different morphologies and enhanced performance in dye-sensitized solar cells

Original Research Article
Pages 69-74
Shibu Zhu, Xiangnan Chen, Feibiao Zuo, Man Jiang, Zuowan Zhou, David Hui

Highlights

► ZnO nanograss with different aspect ratios were synthesized by adjusting PEI content. ► PEI affects both on the aspect ratios and geometrical shapes of ZnO nanograss. ► ZnO nanograss with high aspect ratio and needle-like tip was advantageous for improved photovoltaic conversion performance.

Construction of two novel indium phosphites with (3,6)- and (3,5)-connected frameworks: Synthesis, structure and characterization

Original Research Article
Pages 75-80
Huiduan Li, Lirong Zhang, Qisheng Huo, Yunling Liu

highlights

► Two novel indium phosphite and indium phosphite-oxalate hybrid compounds are synthesized. ► (3, 6)-connected layer structure with **kgd** topology. ► (3,5)-connected binodal net with the Schläfli symbol $(4^2.6)(4^2.6^5.8^3)$.

Synthesis, structures and properties of a series of manganese coordination complexes constructed from dicarboxylic fluorene derivatives

Original Research Article
Pages 81-91

Xing Li, Xiuhua Zhao, Yue Bing, Meiqin Zha, Hongzhen Xie, Zhiyong Guo

Highlights

► Four manganese complexes based on 9,9-diethylfluorene-2,7-dicarboxylic acid were obtained. ► The complexes were structurally characterized by single-crystal X-ray diffraction.

► The complexes 1-4 display different topological structures. ► Thermogravimetric analysis show the complexes have remarkably high thermal stability.

Syntheses, structures and photoelectric properties of a series of Cd(II)/Zn(II) coordination polymers and coordination supramolecules

Original Research Article
Pages 92-102
Jing Jin, Xiao Han, Qin Meng, Dan Li, Yu-Xian Chi, Shu-Yun Niu

Highlights

► Five Cd/Zn complexes have been synthesized and characterized. ► The SPS results indicate they possess obvious photoelectric conversion property. ► The species and coordination environment of central metal ion affect SPS. ► The species and property of ligands affect SPS.

► By the energy-band theory and the crystal filed theory, the SPS are analyzed and assigned.

Phase equilibria, formation, crystal and electronic structure of ternary compounds in Ti–Ni–Sn and Ti–Ni–Sb ternary systems

Original Research Article
Pages 103-112
V.V. Romaka, P. Rogl, L. Romaka, Yu. Stadnyk, N. Melnychenko, A. Grytsiv, M. Falmbigl, N. Skryabina

Highlights

► Ti-Ni-Sn phase diagram was constructed at 1073 K. ► Four ternary compounds are formed: TiNiSn, $TiNi_2$-*x*Sn, Ti_2Ni_2Sn, and Ti_5NiSn_3. ► Three ternary compounds exist in Ti-Ni-Sb system at 873 K. ► The $TiNi_2Sb$ compound is absent.

Nanostructured ceria based thin films (≤1 μ m) As cathode/electrolyte interfaces

Original Research Article
Pages 113-119
J. Hierso, P. Boy, K. Vallé, J. Vulliet, F. Blein, Ch. Laberty-Robert, C. Sanchez

Highlights

► Mesoporous ceria based thin films exhibit interesting performances for Solid Oxide Fuel Cell.

► Mesoporous films were synthesized through the sol–gel process combined with the dip-coating. ► Integrity and connectivity of the nanoparticles facilitates O^{2-} transport across the interface.

Large scale synthesis of nanostructured zirconia-based compounds from freeze-dried precursors

Original Research Article
Pages 120-127
A. Gómez, R. Villanueva, D. Vie, S. Murcia-Mascaros, E. Martínez, A. Beltrán, F. Sapiña, M. Vicent, E. Sánchez

► $Zr1-_xA_xO_{2-x/2}$ *(A=Y,* Sc; $0 \leq x \leq 0.12$) solid solutions have been prepared as nanostructured powders. ► The synthetic method involves the thermal decomposition of precursors obtained by freeze-drying. ► The temperature of the thermal treatment controls particle sizes. ► The preparation procedure has been scaled up to the 100 g scale. ► This method is appropriate for the large-scale industrial preparation of multimetallic systems.

Synthesis, crystal structures and optical properties of two congruent-melting isotypic diphosphates: $LiM_3P_2O_7$ (M=Na, K)

Original Research Article
Pages 128-133
Yunjing Shi, Ying Wang, Shilie Pan, Zhihua Yang, Xiaoyu Dong, Hongping Wu, Min Zhang, Jian Cao, Zhongxiang Zhou

► $LiNa_3P_2O_7$ and $LiK_3P_2O_7$ are new compounds in the Li_2O –M_2O (M=Na, K)-P_2O_5 systems. ►

Highlights

Crystal structures of $LiNa_3P_2O_7$ and $LiK_3P_2O_7$ consist of two-dimensional $[LiP_2O_7]^{3-}$ layers. ► $LiNa_3P_2O_7$ and $LiK_3P_2O_7$ are congruent melting compounds.

Hybrid functional calculation of electronic and phonon structure of $BaSnO_3$

Original Research Article

Highlights

Pages 134-138
Bog G. Kim, J.Y. Jo, S.W. Cheong

Highlights

► We report the full hybrid functional calculation of not only the electronic structure but also the phonon structure for $BaSnO_3$. ► The band gap calculation of HSE06 revealed an indirect gap with 2.48 eV. ► The effective mass at the conduction band minimum and valence band maximum was calculated. ► In addition, the phonon structure of BSO was calculated using the HSE06 functional. ► Finally, the heat capacity was calculated and compared with the recent experimental result.

Investigation on three new metal carboxydiphosphonates: Syntheses, structures, magnetic and luminescent properties

Original Research Article
Pages 139-146
Si-Fu Tang, Xiao-Bo Pan, Xiao-Xia Lv, Xue-Bo Zhao

Highlights

► Three new metal phosphonates were synthesized under hydrothermal conditions. ► Compound **1** exhibits 2D layered structure. ► Compounds **2** and **3** have 1D infinite chain structures. ► Compound **1** displays antiferromagnetic behavior. ► Compounds **2** and **3** show intraligand and ligand to metal charge transfer emission bands.

An X-ray absorption spectroscopic study of the metal site preference in $Al_{1-x}Ga_xFeO_3$

Original Research Article
Pages 147-153
James D.S. Walker, Andrew P. Grosvenor

Highlights

► $Al1-_xGa_xFeO_3$ was investigated by X-ray absorption spectroscopy. ► Ga prefers to occupy the tetrahedral site in $Al1-_xGa_xFeO_3$. ► Fe prefers to occupy the octahedral sites in $Al1-_xGa_xFeO_3$ as *x* increases. ► More anti-site disorder is present in $AlFeO_3$ compared to in $GaFeO_3$.

Rietveld refinement and ionic conductivity of $Ca_{8.4}Bi1._6(PO_4)6O1._8$

Original Research Article
Pages 154-159
I. Tmar Trabelsi, A. Madani, A.M. Mercier, M. Toumi

Highlights

► The Rietveld refinement revealed that the formula of this compound is $Ca_{8.4}Bi1._6(PO_4)6O1._8$.
► Vibrational spectroscopy supports the high symmetry P63/m space group for this apatite.
► This apatite contained channels where oxygen ions were located in 2a sites. ► The possibility of anionic conduction along these channels was considered.

Amine templating effect absent in uranyl sulfates synthesized with 1,4-*n*-butyldiamine

Original Research Article
Pages 160-165
Laurent J. Jouffret, Ernest M. Wylie, Peter C. Burns

Highlights

► Two layered uranyl sulfates were synthesized. ► Amine molecules are located in the interlayers of the compounds. ► No templating effect of the amine was observed. ► Amine molecules are only charge balancing cations in the structures.

Sensitized red luminescence from Mn^{2+}-doped Olgite-type phosphates

Original Research Article
Pages 166-171 Yoshinori
Yonesaki

Highlights

► Olgite-type phosphate red phosphors were prepared by solid state reaction. ► Emission properties of Ce^{3+} doped in $Na_2BaMgP_2O_8$ were investigated. ► Emission properties of Mn^{2+} doped in $Na_2BaMgP_2O_8$ were investigated. ► Crystallographic site occupied by Ce^{3+} and Mn^{2+} ions were spectroscopically identified. ► Energy transfer between Eu^{2+} or Ce^{3+} and Mn^{2+} was investigated for $Na_2BaMgP_2O_8$-based phosphors.

Solid-state synthesis of Mg_2Si via short-duration ball-milling and low-temperature annealing

Original Research Article
Pages 172-180
M. Ioannou, K. Chrissafis, E. Pavlidou, F. Gascoin, Th. Kyratsi

Highlights

► Ball-milling process is crucial for the formation of pure Mg_2Si at low temperatures. ► Synthesis profiles based on different temperature settings and duration are suggested. ► Thermal analysis confirms the shift of the Mg_2Si formation at low temperatures.

Synthesis, structural characterization and high pressure phase transitions of monolithium hydronium sulfate

Original Research Article
Pages 181-185
Debasis Banerjee, Anna M. Plonka, Sun Jin Kim, Wenqian Xu, John B. Parise

Highlights

► A 3-D lithium hydronium sulfate is synthesized by solvothermal methods. ► Two high pressure phase transition occurs due to rotation of sulfate groups. ► The framework undergoes a high temperature structural transformation, to form β-Li_2SO_4 phase.

High temperature synthesis of two open-framework uranyl silicates with ten-ring channels: $Cs_2(UO2)2Si_8O19$ and $Rb_2(UO_2)2Si_5O13$

Original Research Article
Pages 186-190
Jean-Marie Babo, Thomas E. Albrecht-Schmitt

Highlights

► Three-dimensional uranium silicates. ► Analogs of natural uranyl silicate minerals. ► Complexity and symmetry ambiguity of uranyl silicates.

Structural features and enhanced high-temperature oxygen ion transport in $SrFe1-_xTa_xO_{3-}$^

Original Research Article
Pages 191-197
Alexey A. Markov, Elizaveta V. Shalaeva, Alexander P. Tyutyunnik, Vasily V. Kuchin, Mikhail V. Patrakeev, Ilya A. Leonidov, Victor L. Kozhevnikov

The structural studies, oxygen content and conductivity measurements suggest that oxygen depletion from the double perovskite phase constituent of $SrFe1_xTa_xO_3$ ий for x>0.2 is accompanied by formation of pathways for fast ion transport.

Highlights

► The double perovskite type regions are shown to exist in $SrFe1-_xTa_xO_{3-}$. ► The oxygen depletion is accompanied with phase separation. ► The phase separation favors formation of pathways for enhanced oxygen ion transport.

Synthesis, crystal structure and properties of a novel tetra-nuclear Cu complex of ANPyO

Original Research Article
Pages 198-203
Jin-jian Liu, Zu-liang Liu, Jian Cheng

Highlights

► We have synthesized and characterized a new tetra-nuclear Cu complex. ► We have measured its molecular structure and thermal decomposition. ► A special coordination mode between ligand and central copper atoms has been obtained. ► It provides theoretical support to further performance study as energetic catalyst.

Soft chemistry synthesis of high-crystalline orthogermanate $CeGeO_4$: A new photocatalyst

Original Research Article
Pages 204-208
Jun Xing, Chen Yang, Wei Kun Li, Xue Qing Gong, Hua Gui Yang

Highlights

► $CeGeO_4$ as a novel photocatalyst was successfully synthesized by a hydrothermal method. ► Electronic structure and band gap were calculated based on DFT. ► $CeGeO_4$ exhibited a promising photocatalytic performance.

4*f* and 5*d* energy levels of the divalent and trivalent lanthanide ions in $M_2Si_5N_8$ (*M*=Ca, Sr, Ba)

Original Research Article
Pages 209-217
O.M. ten Kate, Z. Zhang, P. Dorenbos, H.T. Hintzen, E. van der Kolk

Highlights

► Construction of energy level schemes of all lanthanides within the $M_2Si_5N_8$ hosts. ► Construction was done by analyzing existing as well as new spectroscopic data. ► Tb^{3+} *d–f* emission from two different Ca sites in $Ca_2Si_5N_8$ has been observed. ► Observation of the Sm^{3+} charge transfer band in $Ca_2Si_5N_8$ and $Sr_2Si_5N_8$. ► Ytterbium has been found in the divalent and trivalent state in $Ca_2Si_5N_8$.

Novel bimetallic thiocyanate-bridged Cu(II)–Hg(II) compounds—synthesis, X-Ray studies and magnetic properties

Original Research Article
Pages 218-227
B. Machura, A. Świtlicka, P. Zwoliński, J. Mroziński, B. Kalińska, R. Kruszynski

Highlights

► Novel heterobimetallic Cu/Hg coordination polymers were synthesised. ► The multidimensional structures have been proved by single X-ray analysIs. ► A variation in the crystalline architectures was observed depending on auxiliary ligands. ► Magnetic measurements indicate weak exchange interaction between Cu(II) in the crystal lattices below 10 K.

Syntheses, crystal structures and characterizations of two new bismuth(III) arsenites

Original Research Article
Pages 228-235
Jun-Hui Liu, Fang Kong, Yan-Li Gai, Jiang-Gao Mao

Highlights

► Solid state reactions of Bi_2O_3 ($BiCl_3$) and As_2O_3 yielded two new phases. ► They represent the first examples of bismuth arsenites. ► The two compounds exhibit two different structural types.

Physical properties of double perovskite-type barium neodymium osmate Ba_2NdOsO_6

Original Research Article

Pages 236-241
Makoto Wakeshima, Yukio Hinatsu, Kenji Ohoyama

Highlights

► Crystal structures of Ba_2NdOsO_6 are determined to be monoclinic below 300 K. ► Its electrical resistivity shows a Mott variable-range hopping behavior with localized carriers. ► An antiferromagnetic ordering of the Os^{5+} moment occurs at 65 K. ► The magnetic structure of Ba_2NdOsO_6 is determined to be of Type I.

Crystal structures and microwave dielectric properties of Zn,W co-

substituted $BaTiO_3$ perovskite ceramics

Original Research Article
Pages 242-247
Cailan Tian, Zhenxing Yue, Yuanyuan Zhou, Longtu Li

Highlights

► A phase transition from simple cubic to hexagonal and then to cubic double pervoskite occurred. ► Refinement results prove that spontaneous dipoles present in face-sharing oxygen octahedra. ► Hexagonal perovskites had higher $Q \times f$, nearer-zero τ_f, and lower ε_r than the cubic ones. ► On the presence of the hexagonal perovskite, $|\tau_f|$ was less than 5 ppm/°C.

The crystal and electronic structures of the $Li_{2-x}Ag_{1+x}In_3$ (x=0.05) indide

Original Research Article
Pages 248-253
Ihor Chumak, Volodymyr Pavlyuk, Grygoriy Dmytriv, Hermann Pauly, Helmut Ehrenberg

Highlights

► The crystal structure of $Li_{2-x}Ag1_{+x}In_3$ has been determined on a single crystal. ► A detailed crystal chemical analysis of $Li_{2-x}Ag1_{+x}In_3$ was performed. ► The electronic structure of the title compound was calculated.

Effects of deformation on the electronic properties of B-C-N nanotubes

Original Research Article
Pages 254-260
S. Azevedo, A. Rosas, M. Machado, J.R. Kaschny, H. Chacham

► We investigated electronic properties of flattened BC_2N nanotubes. ► The electronic states depend strongly on compression. ► It is studied flattened BN nanotubes doped with a carbon atom. ► The flattened C-doped structures, presents a significant reduction of the

Highlights

gap.

Ionothermal synthesis of uranyl compounds that incorporate imidazole derivatives

Original Research Article
Pages 266-272
Ernest M. Wylie, Megan K. Dustin, Jeremy S. Smith, Peter C. Burns

Highlights

► Ionothermal syntheses have produced three new uranyl compounds. ► Imidazole derivatives are incorporated as charge-balancing agents. ► X-ray and spectroscopic analyses reveal variability between imidazole derivatives. ► This method offers synthetic insight in the absence of water at low temperatures.

Thermoelectric transport properties of polycrystalline titanium diselenide *co-intercalated* with nickel and titanium using spark plasma sintering

Original Research Article
Pages 273-278
T.C. Holgate, S. Zhu, M. Zhou, S. Bangarigadu-Sanasy, H. Kleinke, J. He, T.M. Tritt

Highlights

► Single phase bulk Ni and Ti co-intercalated $TiSe_2$ samples prepared by spark plasma sintering. ► Density and X-ray diffraction suggest that the Ni and excess Ti are ordered in the Van der Waals gap. ► Co-intercalation of Ni and Ti can be used to control electron-hole ratio and structural disorder.

Location and oxidation state of iron in Fe-substituted $CuInS_2$ chalcopyrites

Original Research Article
Pages 279-287
Johanna D. Burnett, Tianhong Xu, Monica Sorescu, Brian R. Strohmeier, Jacqueline Sturgeon, Olivier Gourdon, Kristen Baroudi, Jin-lei Yao, Jennifer A. Aitken

Highlights

► X-ray photoelectron spectroscopy confirms the presence of Cu^{+}, In^{3+} and S^{2}-. ► Mössbauer spectroscopy indicates the presence of Fe^{3+}. ► Rietveld refinement of neutron powder diffraction data shows iron on the indium site. ► The band gap decreases to -0.7 eV with only 5% iron substitution. ► Additional characterization is reported.

The synthesis and structure of new transition metal lithium calcium nitride compounds

Original Research Article
Pages 288-296
Janet L. Hunting, Marta M. Szymanski, Amanda L. Kowalsick, Craig M. Downie, Francis J. DiSalvo

Highlights

► Three new lithium calcium nitrides are synthesized. ► Lithium nitride flux used in synthesis.

► Structures contain isolated tetrahedrally coordinated transition metals. ► $Li_{12}Ca_9W_5N_{20}$ contains three crystallographically different W positions.

High temperature structural and magnetic properties of cobalt nanorods

Original Research Article
Pages 297-303
Kahina Ait Atmane, Fatih Zighem, Yaghoub Soumare, Mona Ibrahim, Rym Boubekri, Thomas Maurer, Jérémie Margueritat, Jean-Yves Piquemal, Frédéric Ott, Grégory Chaboussant, Frédéric Schoenstein, Noureddine Jouini, Guillaume Viau

Highlights

► Ferromagnetic Co nanorods are prepared using the polyol process. ► The structural and texture properties of the Co nanorods are preserved up to 500 K. ► The magnetic properties of the Co nanorods are irreversibly altered above 525 K.

DFT+Z7 study of the oxide-ion conductor pentalanthanum hexamolybdenum henicosaoxide

Original Research Article
Pages 304-311
Souraya Goumri-Said, Mohammed Benali Kanoun

Highlights

► Pentalanthanum hexamolybdenum henicosaoxide is an oxide-ion conductor. ► $La_5Mo_6O_{21}$ is metallic with high ionic character due to the presence of oxygen. ► Mo *d*-orbitals are taking the major contribution in the magnetic moment followed by La *f* and then the O *p*-orbitals.

Ca_2Pd_3Ge, a new fully ordered ternary Laves phase structure

Original Research Article
Pages 312-316
Isa Doverbratt, Siméon Ponou, Sven Lidin

Highlights

► Site specific segregation in a Laves phase that is also a Zintl phase. ► Pseudo-gap at the Fermi level in a Laves phase. ► Distorted Frank-Kasper polyhedron.

Ti-71 Interactions and magnetic properties in a series of hybrid inorganic-organic crystals

Original Research Article
Pages 317-322
M. González, A.A. Lemus-Santana, J. Rodríguez-Hernández, M. Knobel, E. Reguera

Highlights

► Hybrid inorganic-organic solids. ► Hybrid inorganic-organic molecular based magnets. ► Ferromagnetic interaction through *TZ–TZ* stacking of imidazole rings. ► Organic pillars formed through *TZ–TZ* stacking.

Calcium-decorated graphyne nanotubes as promising hydrogen storage media: A first-principles study

Original Research Article
Pages 323-328
Yu Sheng Wang, Peng Fei Yuan, Meng Li, Wei Fen Jiang, Qiang Sun, Yu Jia

Highlights

► Ca decorated graphyne nanotubes as hydrogen storage media. ► The gravimetric density of H_2 is 7.44-8.96 wt%. ► The average adsorption energy of hydrogen molecule is 0.13-0.33 eV/H_2. ► It can operate under ambient thermodynamic conditions.

Carbon nanosheet-titania nanocrystal composites from reassembling of exfoliated graphene oxide layers with colloidal titania nanoparticles

Original Research Article
Pages 329-336
Yong-Jun Liu, Mami Aizawa, Wen-Qing Peng, Zheng-Ming Wang, Takahiro Hirotsu

Highlights

► A facile delamination-reassembling method for graphene oxide-titania nanocomposite. ► A nanoporous composite containing mixed phase titania nanocrystals. ► Partition effect of carbon nanosheets preventing TiO_2 nanoparticles from aggregating. ► Adsorption concentration-promoted photocatalysis.

Laser hydrothermal reductive ablation of titanium monoxide: Hydrated TiO particles with modified Ti/O surface

Original Research Article

Highlights

Highlights

► Synthesis of sheet-like β-$Co(OH)_2$ precursors by precipitation method. ► Porous sheet-like Co_3O_4 were obtained by calcining β-$Co(OH)_2$ precursors. ► The possible formation mechanism of porous sheet-like Co_3O_4 has been discussed. ► Porous sheet-like Co_3O_4 decrease the thermal decomposition temperature of ammonium perchlorate.

Highlights

► A chemical-electrochemical method is used to functionalization of SWNTs. ► Functionalization of wall-side of tube is evidenced by anti-Stokes Raman studies. ► FTIR spectra proves insertion of heteropolyanions in polydiphenylamine matrix. ► FTIR spectra of polymer functionalized SWNTs reveal hindrance steric effects.

Ordered nanoporous carbon for increasing CO_2 capture

Original Research Article
Pages 361-365
Hye-Min Yoo, Seul-Yi Lee, Soo-Jin Park

Highlights

► ONCs materials can be prepared readily using the direct-triblock-copolymer-templating method. ► The distributions show that prominent development can be observed around the micro-pore region. ► The soft-templating method provides opportunities for controlling the pore structure of ONCs. ► From thermal power plants for CO2 capture by adsorption technology, is a new direction.

Structure and optical properties of a noncentrosymmetric borate $RbSr_4(BO_3)_3$

Original Research Article
Pages 366-369 M.J. Xia,
R.K. Li

Highlights

► A new noncentrosymmetric borate $RbSr_4(BO_3)_3$ was grown from flux. ► The $RbSr_4(BO_3)_3$ can be viewed as a derivative of the apatite-like structure. ► The structure and its relationship to the optical properties of $RbSr_4(BO_3)_3$ are compared with other NLO crystals with apatite-like structures. ► The basic structural units are the planar BO_3 groups in the structure. ► Second harmonic generation (SHG) test shows that $RbSr_4(BO_3)_3$ can be phase matchable with an effective SHG coefficient about two-thirds as large as that of KH_2PO_4.

Temperature-dependent structural studies of mullite-type $Bi_2Fe_4O_9$

Original Research Article
Pages 370-378
M. Mangir Murshed, Gwilherm Nénert, Manfred Burianek, Lars Robben, Manfred Mühlberg, Hartmut Schneider, Reinhard X. Fischer, Thorsten M. Gesing

Highlights

► Complex expansion–contraction mechanism explains anisotropic thermal expansion. ► Bi $6s^2$ lone electron pair sphericity influences analyses by FTIR autocorrelation. ► Intrinsic effects at 773 K are responsible for extrinsic parameter changes at 900 K.

Step-by-step thermal transformations of a new porous coordination polymer $[(H_2O)_5CuBa(Me_2mal)_2]_n$ (Me_2mal^{2-}=dimethylmalonate): Thermal degradation to barium cuprate

Original Research Article
Pages 379-391
Natalya Zauzolkova, Zhanna Dobrokhotova, Anatoly Lermontov, Ekaterina Zorina, Anna Emelina, Mikhail Bukov, Vladimir Chernyshev, Aleksey Sidorov, Mikhail Kiskin, Artem Bogomyakov, Anton Lytvynenko, Sergey Kolotilov, Yuriy Velikodnyi, Maksim Kovba, Vladimir Novotortsev, Igor Eremenko

Highlights

► New 3D-polymers $[(H_2O)_5CuBa(Me_2mal)_2]n$ and $[(H_2O)CuBa(Me_2mal)_2]n$ were synthesized. ► Thermal analysis showed step-by-step transformations of $[(H_2O)_5CuBa(Me_2mal)_2]n$. ► Crystalline phase of pure cubic $BaCuO_2$ is the product solid-phase thermolysis.

Nanostructured dimagnesium manganese oxide (Spinel): Control of size, shape and their magnetic and electro catalytic properties

Original Research Article
Pages 392-397
Neha Garg, Menaka, Kandalam V. Ramanujachary, Samuel E. Lofland, Ashok K. Ganguli

Highlights

► Mg_2MnO_4 nanorods were synthesized by reverse micellar route. ► Anisotropy of oxalate rods retained in oxides nanorods. ► Nanorods show good catalytic behavior towards oxygen evolution reaction.

Mesoporous VN prepared by solid-solid phase separation

Original Research Article
Pages 398-401
Minghui Yang, Walter T. Ralston, Franck Tessier, Amy J. Allen, Francis J. DiSalvo

► Mesoporous VN has been prepared by solid-solid phase separation. ► Mesoporous VN was characterized by Rietveld refinement of PXRD, SEM and nitrogen physisorption. ► VN materials with different pore sizes (10 nm-50 nm) were synthesized.

Synthesis of metastable rare-earth-iron mixed oxide with the hexagonal crystal structure

Original Research Article
Pages 402-407
Tatsuya Nishimura, Saburo Hosokawa, Yuichi Masuda, Kenji Wada, Masashi Inoue

Highlights

Highlights

► Synthesis of metastable *$REFeO_3$* with hexagonal structure by the co-precipitation method. ► Hexagonal *$REFeO_3$* is obtained for the rare earth elements with small ionic radii. ► Hexagonal-to-orthorhombic transformation of *$REFeO_3$*. ► Catalytic activity of hexagonal

REFeO$_3$ for C_3H_8 combustion.

Spin reorientation and magnetization reversal in the perovskite oxides, $YFe_{1-x}Mn_xO_3$ ($0 \leq x \leq 0.45$): A neutron diffraction study

Original Research Article
Pages 408-413
P. Mandal, C.R. Serrao, E. Suard, V. Caignaert, B. Raveau, A. Sundaresan, C.N.R. Rao

Highlights

► Neutron diffraction study on YFe1-$_x$Mn$_x$O$_3$. ► Spin-reorientation from spin structure Γ_4 to Γ_1. ► Magnetization reversal phenomenon in disordered perovskite oxides, YFe1 $_x$Mn$_x$O$_3$ and YCr $_1$-$_x$Mn$_x$O$_3$. ► Presence of tunable positive and negative magnetocaloric effects in YFe1 $_x$Mn$_x$O$_3$.

$Ce_2AgYb_5/3Se_6$, $La_2CuErTe_5$, and $Ce_2CuTmTe_5$: Three new quaternary interlanthanide chalcogenides

Original Research Article
Pages 414-419
Jean-Marie Babo, Thomas E. Albrecht-Schmitt

Highlights

► New ordered interlanthanide tellurides. ► New quaternary chalcogenides. ► Low-dimensional lanthanide chalcogenide substructures. ► Flux synthesis of new chalcogenides.

Structure refinements of members in the brownmillerite solid solution series $Ca_2Al_x(Fe0.5Mn0._5)_2$-$xO_{5+(5}$ with $1/2 \leq x \leq 4/3$

Original Research Article
Pages 420-428
Stefan Stöber, Günther Redhammer, Susan Schorr, Oleksandr Prokhnenko, Herbert Pöllmann

Highlights

► We present structural data of four Ca-Al-Fe-Mn-brownmillerites. ► Mn^{3+}-ions occupy exclusively the octahedrally coordinated site 0,0,0. ► Bonds and angles of the octahedrally coordinated site are distorted strongly. ► Mn^{3+}-ions influence indirectly the shape of the tetrahedron. ► Mn^{3+}-ions stabilize Pnma instead of I2mb in Ca-Al-Fe-Mn-brownmillerites.

Calorimetric, spectroscopic and structural investigations of phase polymorphism in $[Ru(NH_3)6](BF_4)3$. Part I

Original Research Article
Pages 429-439
Diana Dołęga, Edward Mikuli, Akira Inaba, Natalia Górska, Krystyna Hołderna-Natkaniec, Wojciech Nitek

► Three novel phase transitions are found in $[Ru(NH_3)6](BF_4)_3$. ► The thermodynamic parameters of the phase transitions are derived. ► The transitions are of order-disorder type. ► The complex belongs to *FmJmat* 293 K and its symmetry changes to *1aY* at 170 K. ► $[Ru(NH_3)6](BF_4)_3$ is a highly dynamically disordered crystal.

Electrical and thermal properties of Fe substituted double-filled $Ba_xYb_yFe_zCo4\text{-}_zSb12$ skutterudites

Original Research Article
Pages 440-446
Sedat Ballikaya, Neslihan Uzar, Saffettin Yildirim, James R. Salvador

Highlights

Highlights

► The TE properties of $BaxYb_y$ $FezCo_{4-\ z}Sb_{12}$ compounds were investigated. ► Jonker and Ioffe analysis applied in order to predict the range of power factor achievable at room temperature. ► The thermal conductivity is strongly suppressed with increasing of Fe substitution on Co site. ► We see that small quantities of Fe on Co site is beneficial on enhancement *ZT* value.

Crystal structure, morphotropic phase transition and luminescence in

the new cyclosilicates $Sr_3R_2(Si_3O_9)_2$, R=Y, Eu-Lu

Original Research Article
Pages 447-455
Alexander P. Tyutyunnik, Ivan I. Leonidov, Ludmila L. Surat, Ivan F. Berger, Vladimir G. Zubkov

Highlights

► A new group of cyclosilicates $Sr_3R_2(Si_3O_9)_2$, R=Y, Eu-Lu, was first synthesized. ► Isolated $[Si_3O_9]$ rings located in layers are basic building units and stack with Sr/R layers along the [1 0 **7**] direction. ► The rare earth atoms are distributed among three independent Sr/R sites coordinated by 6, 7 and 8 oxygen ligands. ► A step-like change of the unit cell parameters is observed in the $Sr_3R_2(Si_3O_9)_2$ structure for R=Er→Tm.► $Sr_3Y_2(Si_3O_9)_2:Eu^{3+}$ demonstrates intense multiband orange-red photoluminescence.

Copper uranyl phosphate and arsenate incorporating an organic ligand with a pillared layer structure: $[Cu(4,4'\text{-bpy})(UO_2)_{0.5}(HPO_4)(H_2PO_4)]H_2O$ and [Cu(4,4′-

bpy)(UO_2)05(HAsO4)(H_2AsO4)]1.5H2O

Original Research Article
Pages 456-459
Chih-Min Wang, Kwang-Hwa Lii

.

Analysis of the magnetic corrosion product deposits on a boiling water reactor cladding

Original Research Article
Pages 460-465
Andrey Orlov, Claude Degueldre, Wilfried Kaufman

Analysis of spinels in corrosion product deposits on boiling water reactor fuel rod. Combining EPMA and XAFS results: schematic representation of the ferrite spinels in terms of the end members and their extent of inversion. Note that the ferrites are represented as a surface between the normal (upper plane, $M[Fe_2]O_4$) and the inverse (lower plane, $Fe[MFe]O_4$).

Actual compositions

red for the specimen at low elevation (810 mm),

blue for the specimen at mid elevation (1800 mm).

The results have an impact on the properties of the CRUD material.

Highlights

► Buildup of corrosion product deposits on fuel claddings of a boiling water reactor (BWR) are investigated. ► Under BWR water conditions, Zn addition with Ni and Mn induced formation of (Zn,Ni,Mn)[Fe_2O_4]. ► X-Ray Adsorption Spectroscopy (XAS) revealed inversion of cations in spinel solid solutions. ► Zinc-rich ferrite spinels are formed on BWR fuel cladding mainly at lower pin elevations.

Structure of $Li_4B_2O_5$: High-temperature monoclinic and low-temperature orthorhombic forms

Original Research Article
Pages 466-470
Meng He, Hiroki Okudera, Arndt Simon, J. Köhler, Shifeng Jin, Xiaolong Chen

Highlights

► Structures of two polymorphs of $Li_4B_2O_5$ are determined. ► The high and low temperature phases are monoclinic and orthorhombic, respectively. ► A slight larger molar volume was observed for the low temperature phase. ► Symmetry elements are lost in the phase transition from high to low temperature.

Synthesis and crystal structure of $Mg_{0.5}NbO_2$: An ion-exchange reaction with Mg^{2+} between trigonal $[NbO_2]$" layers

Original Research Article
Pages 471-474
Akira Miura, Takahiro Takei, Nobuhiro Kumada

Highlights

► A new layered niobate, $Mg_{0.5}NbO_2$, was synthesized from $LiNbO_2$. ► Cation-exchange reaction converted two monovalent Li^+ into one divalent Mg^{2+} at 450-550 °C. ► $Mg_{0.5}NbO_2$ was isostructural with $LiNbO_2$ (space group; *$P6_3$/ mmc).* ► Its lattice parameters were *a*=2.9052(6) Å and *c*=10.625(15) Å. ► Synthesized $Mg_{05}NbO_2$ was calculated to be thermodynamically more favorable.

Controlling structure distortions in 3-layer ferroelectric Aurivillius oxides

Original Research Article
Pages 475-482
Eric J. Nichols, Jiawanjun Shi, Ashfia Huq, Sven C. Vogel, Scott T. Mistur

Highlights

► *A*-site cations define the tilt and distortion of the octahedral. ► Distortions of oxygen octahedra, ignoring the central cation, link to ferroelectric polarization. ► Bi ion occupancy in the perovskite causes distortion of the oxygen sublattice. ► We predict multiferroic behavior from off-centering caused by the Bi ion lone pair.

Copper(II)–lanthanide(III) coordination polymers constructed from pyridine-2,5-dicarboxylic acid: Preparation, crystal structure and photoluminescence

Original Research Article
Pages 489-498
Zheng-Qiang Xia, Qing Wei, San-Ping Chen, Xin-Ming Feng, Gang Xie, Cheng-Fang Qiao, Guo-Chun Zhang, Sheng-Li Gao

Highlights

► Seven 3d-4f heterometallic compounds have been prepared and characterized. ► **1**-**5** and **7** are constructed from $Ln_2Cu_2L_2(H_2O)_2$ rings and $CuL_2(H_2O)$ building blocks. ► One new coordination mode of the $pydc^{2-}$ ligand is first observed. ► **1**-**2** exhibit intense characteristic luminescence emission spectra of lanthanide ions.

Influence of biphenyl spacer appended to the flexible phosphonate arms in modulating the dimensionality of the coordination polymers: Synthesis, structural chemistry and magnetic properties

Original Research Article
Pages 499-507
Bharat Kumar Tripuramallu, Samar K. Das

Highlights

► Cobalt containing coordination polymer and a nickel discrete compound have been synthesized. ► Flexible ligand 4,4'-dimethylenebiphenyldiphosphonic acid has been employed. ► Co(II) and Ni(II) ions are square pyramidal and octahedral respectively. ► The effect of the twisting in the benzene rings in the associated ligand has been demonstrated.

In situ dehydration behavior of zeolite-like pentagonite: A single-crystal X-ray study

Original Research Article
Pages 508-516
Rosa Micaela Danisi, Thomas Armbruster, Biljana Lazic

Highlights

► We investigate the relationship between the removal of H_2O molecules and structural modifications of the framework of pentagonite. ► Pentagonite undergoes phase transitions upon heating. ► We analyze similarities and differences between pentagonite and related structures.

Functionalization of multi-walled carbon nanotubes using water-assisted chemical vapor deposition

Original Research Article
Pages 517-522
Maofei Ran, Wenjing Sun, Yan Liu, Wei Chu, Chengfa Jiang

Highlights

► MWCNTs were functionalized by water-assisted CVD method. ► Defects and weak-medium acidic sites were created on the MWCNT sidewalls. ► Oxygen-containing groups in

functionalized MWCNT were increased from 21.1% to 42%. ► A mechanism for the influence of water vapor on MWCNTs was proposed.

Magnetic and electrical properties of flux grown single crystals of $Ln_6M_4Al_{43}$ (*Ln*=Gd, Yb; *M*=Cr, Mo, W)

Original Research Article
Pages 523-531
Michael J. Kangas, LaRico J. Treadwell, Neel Haldolaarachchige, Jacob D. McAlpin, David P. Young, Julia Y. Chan

Highlights

► Single crystals up to 0.5 cm in length were grown with a molten aluminum flux. ► Physical property measurements were conducted on single crystals. ► Gadolinium analogs appear to order antiferromagnetically with positive θ. ► All analogs show metallic resistivity.

An investigation of the electronic structure of Cu_2FeSn_3-xTi_xS_8 ($0 \leq x \leq 3$) thiospinel spin-crossover materials by X-ray absorption spectroscopy and electronic structure calculations

Original Research Article
Pages 532-542
John R. Hayes, Andrew P. Grosvenor

Highlights

► Cu_2FeSn_3-xTi_xS_8 thiospinels were investigated by XANES. ► The covalency of the Fe-S and Ti-S bonds increases with greater Ti incorporation. ► *T*-dependent Fe K-edge XANES spectra were collected to investigate SCO transitions. ► Covalent bonding makes study of the SCO transition difficult by Fe K-edge XANES. ► The bonding interactions were investigated through examination of S K-edge spectra.

Synthesis, crystal structure, and properties of $KSbO_3$-type Bi3Mn19Te11O11

Original Research Article
Pages 543-549
Man-Rong Li, Maria Retuerto, Yong Bok Go, Thomas J. Emge, Mark Croft, Alex Ignatov, Kandalam V. Ramanujachary, Walid Dachraoui, Joke Hadermann, Mei-Bo Tang, Jing-Tai Zhao, Martha Greenblatt

► High pressure Bi_3Mn_3O11 is stabilized by partial Te substitution at ambient pressure. ► New $KSbO_3$-type $Bi3Mn1.9Te1.1O_{11}$ single crystal was grown from binary flux. ► The presence of

Highlights

mixed oxidation state of manganese is evidenced by XANES study. ► The Te-substitution destroys the long-range magnetic ordering and relaxes the structure.

Atomistic calculations of the thermodynamic properties of mixing for tetravalent metal dioxide solid solutions: (Zr, Th, Ce)O_2

Original Research Article
Pages 550-559
L.C. Shuller-Nickles, R.C. Ewing, U. Becker

Highlights

► ΔH_{mx}, ΔG_{mx}, and ΔS_{mx} of $Th_xCe1_{\ x}O_2$, $Th_xZr_{1-x}O_2$, and $Ce_xZr_{1\ x}O_2$ binaries are calculated. ► Cation ordering is identified at low *T* for binaries containing ZrO_2. ► Phase diagrams are estimated based on DFT and Monte-Carlo calculations. ► DFT and Monte-Carlo calculations are in agreement with experimental (and previous computational) results, where available. ► Increased thermodynamic stability of monoclinic and tetragonal ZrO_2 end-member affects solid solution binaries.

Microwave assisted hydrothermal synthesis of Ag/AgCl/WO_3

photocatalyst and its photocatalytic activity under simulated solar light

Original Research Article
Pages 560-565
Rajesh Adhikari, Gobinda Gyawali, Tohru Sekino, Soo Wohn Lee

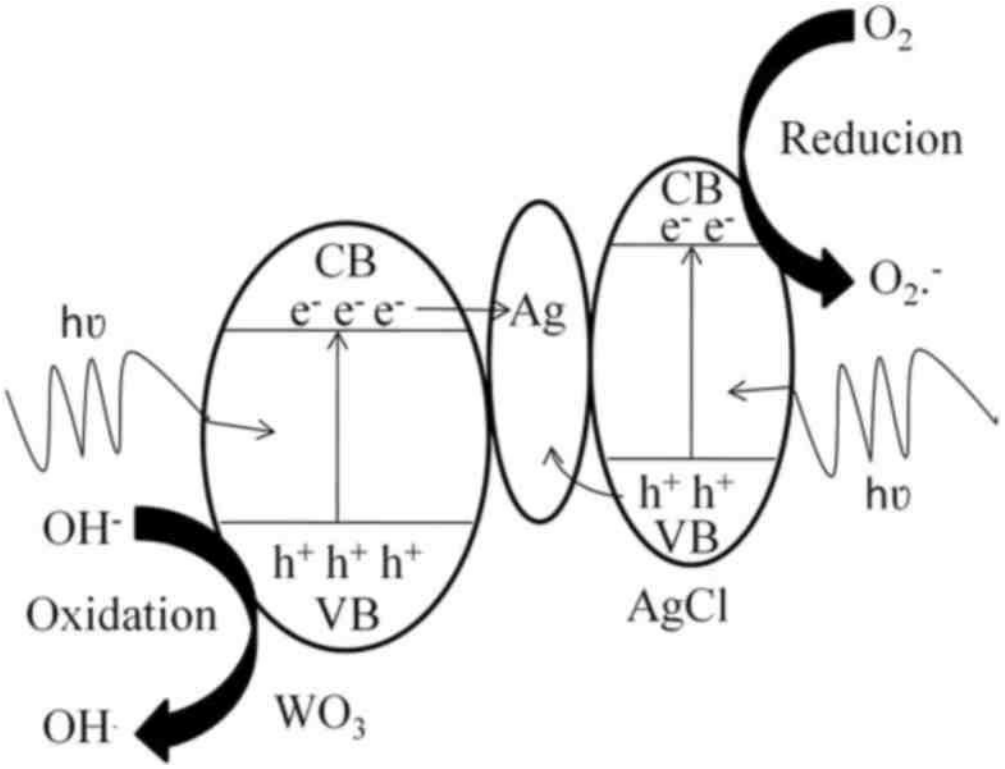

Highlights

► Successful synthesis of Ag/AgCl/WO_3 nanocomposite. ► Photocatalytic experiment was performed under simulated solar light. ► Nanocomposite photocatalyst was very active as compared to WO_3 commercial powder. ► SPR effect due to Ag nanoparticles enhanced the photocatalytic activity. Rapid Communications

Synthesis of MOF having hydroxyl functional side groups and optimization of activation process for the maximization of its BET surface area

Pages 261-265
Jongsik Kim, Dong Ok Kim, Dong Wook Kim, Kil Sagong

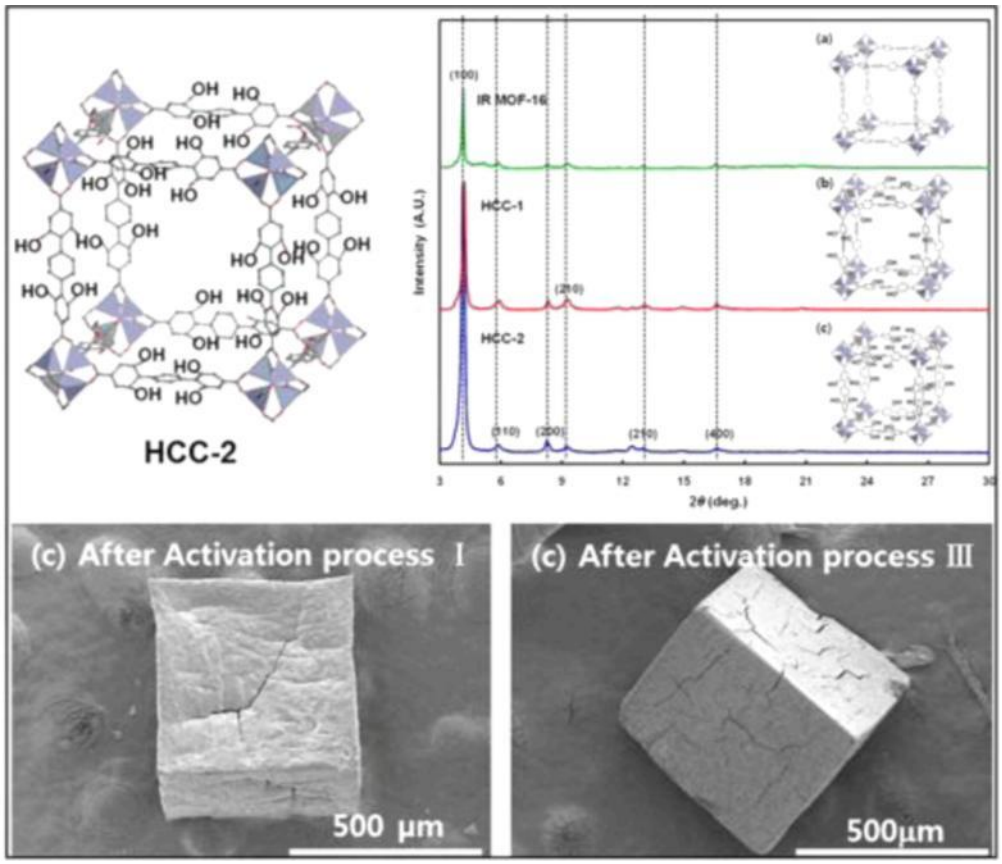

Highlights

► HCC-2 having higher number of hydroxyl groups than that of HCC-1 was prepared. ► The optimization of activation process for HCC-2 was studied. ► The crystal structure of HCC-2 was a cubic-shaped structure with each axis of 21.5 Å. ► -OH functionalities on HCCs had negative influence on their H_2 adsorption abilities. ► This might be due to impurities rigidly attached to their functional side groups.

Synthesis and characterization of nano ZnO rods via microwave assisted chemical precipitation method

Pages 483-488
N. Uma Sangari, S. Chitra Devi

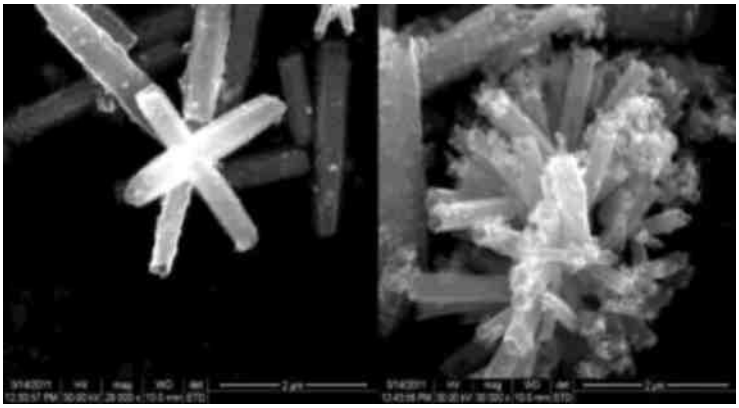

Highlights

► Increase in alkalinity of the precursor solution results in longer rods. ► Beyond a saturation limit, the excess of added OH- ions inhibited the growth of rods. ► Keeping all parameters the same, the alkalinity can only modify the aspect ratio of the rods and not their morphology.